

Coupling of fully Eulerian and arbitrary Lagrangian–Eulerian methods for fluid-structure interaction computations

Thomas Wick

Received: 18 January 2013 / Accepted: 22 April 2013 / Published online: 8 May 2013
© Springer-Verlag Berlin Heidelberg 2013

Abstract We present a specific application of the fluid-solid interface-tracking/interface-capturing technique (FSITICT) for solving fluid-structure interaction. Specifically, in the FSITICT, we choose as interface-tracking technique the arbitrary Lagrangian–Eulerian method and as interface-capturing technique the fully Eulerian approach, leading to the Eulerian-arbitrary Lagrangian–Eulerian (EALE) technique. Using this approach, the domain is partitioned into two sub-domains in which the different methods are used for the numerical solution. The discretization is based on a monolithic solver in which finite differences are used for temporal integration and a Galerkin finite element method for spatial discretization. The nonlinear problem is treated with Newton’s method. The method combines advantages of both sub-frameworks, which is demonstrated with the help of some benchmarks.

Keywords Finite elements · Fluid-structure interaction · Monolithic formulation · Arbitrary Lagrangian–Eulerian approach · Fully Eulerian approach

Mathematics Subject Classification (2000) 65N30 · 65M60 · 74F10

1 Introduction

For computing fully nonstationary fluid-structure interactions, we propose a specific realization of the fluid-solid interface-tracking/interface-capturing technique (FSITICT) [1], which itself is the fluid-structure interaction (FSI) version of the mixed interface-tracking/interface-capturing technique (MITICT) [2]. These methods are used for the numerical solution of multiphysics problems in non-overlapping domains. Specifically, the computational domain is partitioned into two (but fixed) sub-domains. In one domain using an interface-tracking method and in the other one an interface-capturing method. Using FSITICT in this study, we employ specifically as interface-tracking approach the arbitrary Lagrangian–Eulerian (ALE) method [3–6] and as interface-capturing method the fully Eulerian (E) approach [7,8] that is based on a level-set like initial point set. This specific choice in the FSITICT leads to the Eulerian-arbitrary Lagrangian–Eulerian (EALE) framework, first introduced in [9] for solving steady-state FSI and computational structure mechanics (CSM). To the best of our knowledge, we have not seen in the literature any application of (such as the EALE method) or test computations with the FSITICT. Consequently, we are going to explore important aspects and results in this study.

As previously mentioned, a coupling of interface-tracking and interface-capturing methods has previously been proposed for the coupling of fluid flows given by different methods [10,1]. The MITICT method was originally introduced to compute fluid-object interactions with multiple fluids. It was successfully tested in [11,12] by computing numerical tests for a collapse of a cylindrical water column and interaction of a fluid with an oscillating cylinder. In those studies, the DSD/SST formulation (see, e.g., [13–17]) is used as interface-tracking method. Adding an

T. Wick (✉)
The Institute for Computational Engineering and Sciences,
The University of Texas at Austin, Austin, TX 78712, USA
e-mail: twick@ices.utexas.edu

T. Wick
Institute for Applied Mathematics, Heidelberg University,
INF 293/294, 69120 Heidelberg, Germany
e-mail: thomas.wick@iwr.uni-heidelberg.de

additional advection equation to the DSD/SST formulation for the time-evolution of the interface can be handled with an interface-capturing method such as the enhanced-discretization interface-capturing technique (EDICT) [18, 19] or the edge-tracked interface locator technique (ETILT) [2, 1].

Turning back to the present work, a typical application of the EALE approach are heart valve simulations, which is quite often of interest [20–25]. Here, the leaflets (classified as a first structure immersed in blood flow) might meet at the tips. In fact an Eulerian description of elasticity allows for (very) large deformations and contact. Both issues have to be considered when performing valve simulations. On the other hand, the elastic walls of the aorta (described as second elastic structure) are typically located on boundary parts of the computational domain for which the ALE method as a mesh-moving approach is preferable.

The numerical solution of the EALE method is obtained with a monolithic solution algorithm in which each sub-framework is treated with a monolithic solution algorithm itself; for monolithic ALE, we refer the reader in particular to Hron [26, 27], Huebner et al. [28], Bazilevs et al. [29], and to the book [30]. Moreover, quasi-direct and direct coupling methods allowing non-matching grids at the interface have been proposed in [31, 32]. Specifically, these methods reduce to a standard monolithic scheme if the grids are matching. For monolithic Eulerian (for which a lot of work has been done in recent years), we mention the following studies performed by Dunne, Richter, and Wick [7, 33–35]. Apart from monolithic formulations, other recent studies on fully Eulerian formulations are known [36–40].

The reason to test a monolithic solver is motivated by the fact that we need an algorithm of strong coupling type for future applications in computational medicine because therein, fluid and structure densities are of the same order and thus the added-mass effect becomes important [41]. It has been shown that a monolithic solver should be preferred in such cases [42]. This is in fact the main reason to formulate both fluid in structure in the same coordinates. Since we like to avoid any transformation in the fluid (keeping it in Eulerian coordinates), we need to reformulate the elastic structure also in the same system. In fact, a structure description in the same dimension as the fluid is a key difference to other studies.

The numerical discretization can be done independently for each sub-framework and therefore, standard algorithms can be applied. In detail, the temporal discretization is based on finite differences and spatial discretization is done using a standard Galerkin finite element approach in which pure hyperbolic terms are stabilized by some diffusion. The solution of the nonlinear system can be achieved with a Newton method, which is very attractive because it provides robust and rapid convergence. The Jacobian matrix is derived by exact linearization which is demonstrated for our settings

in [43, 44, 35]. Because the development of iterative linear solvers is difficult for fully coupled problems, specifically for fluid-structure interaction in fully Eulerian coordinates, we restrict ourselves to use a direct solver (UMFPACK [45]).

The organization of the article is as follows. We begin by introducing notation, transformation rules between Eulerian and Lagrangian coordinates and finally, the governing equations in their natural coordinate systems. In the third Section, the EALE setting for computing fully nonstationary fluid-structure interaction is given. Next, in Sect. 4, a brief account on the discretization is provided to the reader. Finally, some numerical tests are used to substantiate our theoretical findings. The framework is validated with comparison to the steady-state framework [9] and by studies to spatial and temporal mesh convergence. The examples are computed with an extension of our ALE solver [46] that is build upon the software library deal. II [47].

2 Notation, transformations, and equations

In this section, we explain the idea of the EALE approach and the (possible) partitioning of the computational domain in Fig. 1. Afterwards, more notation, transformation rules between Lagrangian and Eulerian coordinates and finally, the governing equations in their natural coordinates are introduced.

2.1 Notation

Let $\Omega \subset \mathbb{R}^2$ be a polygonal domain. This domain is split into two non-overlapping subdomains $\Omega_f(t)$ and $\Omega_s(t)$ with a common interface $\Gamma_i(t)$. The outer boundaries are denoted by $\partial\Omega_f(t)$ and $\partial\Omega_s(t)$, respectively. In the initial configuration at time step $t = 0$, the structure is located in $\Omega_s(0)$; the same holds for the fluid. Throughout this study, we indicate with ‘f’ and ‘s’ suffixes, fluid- and structure-related terms, respectively.

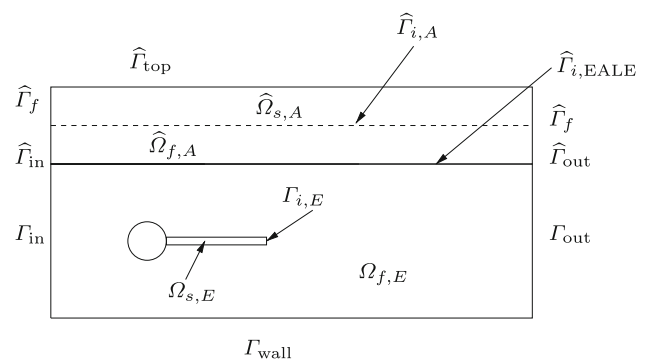


Fig. 1 Prototypical configuration for the coupling of ALE coordinates with fully Eulerian coordinates

The initial (or later reference) domains are denoted by $\widehat{\Omega}_f$ and $\widehat{\Omega}_s$, respectively. Furthermore, we denote the outer boundary by $\partial\widehat{\Omega} = \widehat{\Gamma} = \widehat{\Gamma}_D \cup \widehat{\Gamma}_N$ where $\widehat{\Gamma}_D$ and $\widehat{\Gamma}_N$ denote Dirichlet and Neumann boundaries, respectively. For the convenience of the reader and when we expect no confusion, we omit the explicit time-dependence and we use $\Omega := \Omega(t)$ to indicate time-dependent domains. If necessary, we distinguish the Eulerian and the ALE domain for fluid flows via $\Omega_{f,E}$ and $\widehat{\Omega}_{f,A}$. In a similar way we distinguish the structural domains. It holds,

$$\widehat{\Omega} := \Omega_E \cup \widehat{\Omega}_A = \Omega_{f,E} \cup \Omega_{s,E} \cup \widehat{\Omega}_{f,A} \cup \widehat{\Omega}_{s,A}.$$

The Eulerian and the ALE domain will be coupled on the common fluid interface $\widehat{\Gamma}_{i,EALE} = \partial\Omega_{f,E} \cap \partial\widehat{\Omega}_{f,A}$. The other interfaces are denoted by $\widehat{\Gamma}_{i,A} = \partial\widehat{\Omega}_{f,A} \cap \partial\widehat{\Omega}_{s,A}$ and $\Gamma_{i,E} = \partial\Omega_{f,E} \cap \partial\Omega_{s,E}$.

We adopt standard notation for the usual Lebesgue and Sobolev spaces [48,49]. Let $X \subset \mathbb{R}^d$, $d = 2, 3$ be a time-independent domain. For instance, we later use $X := \Omega_f$ or $X := \Omega_s$. Specifically, we define $H_0^1(X) = \{u \in H^1(X) : u = 0 \text{ on } \Gamma_D \subset \partial X\}$. We use frequently the short notation

$$V_X := H^1(X), \quad V_X^0 := H_0^1(X), \tag{1}$$

$$L_X := L^2(X), \quad L_X^0 := L^2(X)/\mathbb{R}. \tag{2}$$

Specifically, we introduce the trial and the test space of the velocity variables in the fluid domain,

$$V_{f,v}^0 := \{v_f \in H_0^1(\Omega_f) : v_f = v_s \text{ on } \Gamma_i\}. \tag{3}$$

Moreover, we introduce the trial and the test spaces for the moving-mesh displacement in the fluid domain,

$$V_{f,u}^0 := \{u_f \in H_0^1(\Omega_f) : u_f = u_s \text{ on } \Gamma_i\}, \tag{4}$$

$$V_{f,u,\Gamma_i}^0 := \{\psi_f \in H_0^1(\Omega_f) : \psi_f = 0 \text{ on } \Gamma_i\}. \tag{5}$$

Analogously, we define the respecting ‘hat’ spaces for the ALE coordinates by defining the spaces on $\widehat{X} := \widehat{\Omega}_f$ or $\widehat{X} := \widehat{\Omega}_s$. Finally, the time interval is denoted by $I_T := [0, T]$ with the end-time value T .

2.2 Transformation rules

Let us briefly recapitulate the necessary ingredients to transform variables, vectors, and tensors from Eulerian to Lagrangian systems and vice versa. The ALE mapping is defined in terms of the fluid mesh displacement \hat{u}_f such that

$$\hat{\mathcal{A}}(\hat{x}, t) : \widehat{\Omega}_f \times I_T \rightarrow \Omega_f, \quad \text{with } \hat{\mathcal{A}}(\hat{x}, t) = \hat{x} + \hat{u}(\hat{x}, t). \tag{6}$$

It is specified through the deformation gradient and its determinant

$$\widehat{F} := \widehat{\nabla} \hat{\mathcal{A}} = \hat{I} + \widehat{\nabla} \hat{u}, \quad \hat{J} := \det(\widehat{F}). \tag{7}$$

Furthermore, function values in Eulerian and Lagrangian coordinates are identified by

$$u(x) =: \hat{u}(\hat{x}), \quad \text{with } x = \hat{\mathcal{A}}(\hat{x}, t). \tag{8}$$

The mesh velocity is defined by $\partial_t \hat{\mathcal{A}}$. Next, we define the inverse transformation required for the fully Eulerian framework, which is, however, only required in the structure domain Ω_s :

$$\mathcal{A}(x, t) : \Omega_s \times I_T \rightarrow \widehat{\Omega}_s, \quad \text{with } \mathcal{A}(x, t) = x - u_s(x, t). \tag{9}$$

Simple calculation yields [7]:

$$\mathcal{A}(\hat{\mathcal{A}}(\hat{x}, t), t) = \hat{x}. \tag{10}$$

Spatial differentiation of (10) brings us

$$(I - \nabla u_s) \underbrace{(\hat{I} + \widehat{\nabla} \hat{u}_s)}_{=\widehat{F}_s} = \hat{I}, \tag{11}$$

where I and \hat{I} denote the identity matrices. The following relations between the ALE deformation gradient and its Eulerian counterpart can be inferred from the previous calculations:

$$\widehat{F}_s = (\hat{I} + \widehat{\nabla} \hat{u}_s) = (I - \nabla u_s)^{-1} =: F_s^{-1}, \tag{12}$$

$$\hat{J}_s = \det(\widehat{F}_s) = \det(F_s^{-1}) =: J_s^{-1}. \tag{13}$$

Summarizing, we obtain the deformation gradient and its determinant in Eulerian coordinates:

$$F_s = (I - \nabla u_s), \quad J_s := \det(F_s). \tag{14}$$

Remark 1 In the same way, we define F_f and J_f in the fluid part.

Remark 2 In the following, we use the short hand notation F and J because it is clear from the context whether we work with F_s and J_s or F_f and J_f , respectively.

With the help of these relations, we recapitulate the Green-Lagrange tensors in both coordinate systems:

$$E := \frac{1}{2} (F^{-T} F^{-1} - I), \quad \widehat{E} := \frac{1}{2} (\widehat{F}^T \widehat{F} - \hat{I}). \tag{15}$$

With the previously definitions, we recall the constitutive stress tensors in the respective frameworks:

$$\sigma_f := \sigma_f(v_f, p_f) = -p_f I + 2\rho_f v_f (\nabla v_f + \nabla v_f^T), \tag{16}$$

$$\widehat{\sigma}_f := \widehat{\sigma}_f(\hat{v}_f, \hat{p}_f) = -\hat{p}_f \hat{I} + 2\hat{\rho}_f v_f (\widehat{\nabla} \hat{v}_f \widehat{F}^{-1} + \widehat{F}^{-T} \widehat{\nabla} \hat{v}_f^T), \tag{17}$$

with the velocity v_f , the pressure p_f , the density ρ_f , and the (kinematic) viscosity v_f and their respective ‘hat’ coordinates for the definition in the ALE framework. For elastic

structures, we use the laws based on the Saint Venant-Kirchhoff (STVK) material:

$$\sigma_s := \sigma_s(u_s) = JF^{-1}(\lambda_s(\text{tr}E)I + 2\mu_s E)F^{-T}, \tag{18}$$

$$\widehat{\sigma}_s := \widehat{\sigma}_s(\widehat{u}_s) = \widehat{J}^{-1}\widehat{F}(\lambda_s(\text{tr}\widehat{E})\widehat{I} + 2\mu_s \widehat{E})\widehat{F}^T, \tag{19}$$

in which the material is characterized by the Lamé coefficients λ_s and μ_s .

It remains to recall the concept of time-derivatives in both frameworks. As before, let $x = x(\widehat{x}, t)$, where \widehat{x} denotes the initial position of the point x . The velocity v is defined as the total time derivative of the point's position:

$$v(x, t) = d_t x(\widehat{x}, t). \tag{20}$$

In Lagrangian coordinates, the total time derivative of a function $\widehat{u}(\widehat{x}, t) := u(x(\widehat{x}, t), t)$ is determined by

$$d_t \widehat{u}(\widehat{x}, t) = \partial_t \widehat{u}(\widehat{x}, t) + \widehat{\nabla} \widehat{u}(\widehat{x}, t) d_t \widehat{x} = \partial_t \widehat{u}(\widehat{x}, t), \tag{21}$$

or short

$$d_t \widehat{u} = \partial_t \widehat{u}, \tag{22}$$

because $d_t \widehat{x} = 0$ in the Lagrangian system. In contrast, the total time derivative of a function $u(x, t)$ in the Eulerian framework reads:

$$\begin{aligned} d_t u(x, t) &= \partial_t u(x, t) + \nabla u(x, t) d_t x \\ &= \partial_t u(x, t) + \nabla u(x, t) v(x, t) \\ &= \partial_t u(x, t) + v(x, t) \cdot \nabla u(x, t). \end{aligned} \tag{23}$$

Or short:

$$d_t u = \partial_t u + v \cdot \nabla u. \tag{24}$$

The convection term $v \cdot \nabla u$ denotes the key difference between time derivatives in both frameworks and plays an important role when formulating the governing elasticity equations in Eulerian coordinates.

2.3 Governing equations in their natural coordinates

We start by recalling the fluid flows modeled by the Navier-Stokes equations [2] in a suitable domain and some initial and boundary conditions:

Problem 1 Find fluid's velocity v_f and fluid's pressure p_f such that

$$\begin{aligned} \rho_f \partial_t v_f + \rho_f v_f \cdot \nabla v_f - \text{div} \sigma_f &= 0, \\ \text{div} v_f &= 0, \end{aligned} \tag{25}$$

in which $\sigma_f = -p_f I + \rho_f v_f (\nabla v_f + \nabla v_f^T)$ denotes fluid's Cauchy stress tensor and finally, ρ_f and v_f the density and viscosity, respectively.

The second order in time hyperbolic equations for modeling elastic structures in some suitable domain with initial and boundary conditions read [50]:

Problem 2 Find structure's displacement \widehat{u}_s such that:

$$\widehat{\rho}_s d_t^2 \widehat{u}_s - \widehat{\text{div}}(\widehat{J} \widehat{\sigma}_s \widehat{F}^{-T}) = 0, \tag{26}$$

or equivalently find \widehat{u}_s and the velocity \widehat{v}_s :

$$\widehat{\rho}_s d_t \widehat{v}_s - \widehat{\text{div}}(\widehat{J} \widehat{\sigma}_s \widehat{F}^{-T}) = 0, \tag{27}$$

$$d_t \widehat{u}_s - \widehat{v}_s = 0, \tag{28}$$

in which the constitutive tensor reads $\widehat{J} \widehat{\sigma}_s \widehat{F}^{-T} := \widehat{F} \widehat{\Sigma}_s = \widehat{F}(\lambda_s(\text{tr}\widehat{E})\widehat{I} + 2\mu_s \widehat{E})$.

Both systems are completed with boundary conditions that are later specified.

Remark 3 Formulating Eq. 27 in Eulerian coordinates changes its type to a pure hyperbolic model, which requires numerical stabilization for discretization. Details are found in [35].

Finally, we introduce the initial point set (IPS) [7] for the fully Eulerian framework. This equation is defined on the continuous level (like a level-set function) and is used (after discretization) to map each structure point to its initial position:

Problem 3 Find u such that

$$\partial_t u - w + (w \cdot \nabla)u = 0, \tag{29}$$

The initial and boundary conditions are given by

$$\begin{aligned} u(x, 0) &= 0, \quad x \in \Omega_E, \\ u(x, t) &= 0, \quad x \in \partial\Omega_E, \quad t \in I_T. \end{aligned}$$

Then, the value of u is transported with the velocity w to its initial position at time zero.

Remark 4 (Difference of the IPS-function and a level-set-function) Using the IPS-function, the position of the interface is determined by structural mechanics. In contrast, a level-set-function is given by the local fluid velocity normal to the interface.

The EALE approach is now based on the following steps:

- Formulate a coupled problem in ALE coordinates in the domain $\widehat{\Omega}_A$, i.e., reformulate the flow equations in a fixed arbitrary reference configuration and keep the structure deformations in Lagrangian coordinates.
- Formulate a coupled problem in fully Eulerian coordinates in the domain Ω_E , i.e., keep the fluid equations in the Eulerian system and reformulate structural deformations in Eulerian coordinates.
- Formulate the both previous frameworks into one single variational monolithically-coupled formulation.

In the remainder of this study, a framework for computing *nonstationary* processes is presented. This is a key extension to another study [9] in which steady-state processes are taken into consideration. In fact, nonstationary processes require careful consideration of numerical issues that shall be discussed in the next two sections.

3 The EALE method for fully nonstationary processes

To organize a fully monolithically-coupled formulation, the computational domain $\widehat{\Omega}$ is split into an ALE subdomain and an Eulerian subdomain, i.e., $\widehat{\Omega} = \widehat{\Omega}_A \cup \Omega_E$ as explained in Sect. 2.1.

Using partial integration to derive a weak setting, and transformation to a reference configuration, a common setting for fluid flows and structural deformations is obtained. For computations with moderate velocities, the effect of convection can be neglected as explained in [9]. This is a simplification of crucial importance. In fact, fluid flows with high velocities (but still laminar), the choice $w := v_f$ leads to smear-off effects which are well-known in the level-set community. Since we are interested in a consistent variational formulation without performing a sub-time step procedure for reinitialization [51], we extend v_f harmonically [7,35]. Specifically,

$$w = v_s \quad \text{in } \Omega_{s,E} \cup \Gamma_{i,E}, \tag{30}$$

$$\Delta w = 0 \quad \text{in } \Omega_{f,E}. \tag{31}$$

With the help of this additional equation, we propose the following EALE framework for computing fully nonstationary processes:

Problem 4 (Variational fluid-structure interaction in EALE coordinates with an additional velocity) Find the following variables:

- Velocities $\{v_f, \hat{v}_f, v_s, \hat{v}_s\} \in \{v_f^D + V_{f,v}^0\} \times \{\hat{v}_f^D + \hat{V}_{f,\hat{v}}^0\} \times \{v_s^D + V_{s,v}^0\} \times \hat{L}_s$ with $v_f(0) = v_f^0, \hat{v}_f(0) = \hat{v}_f^0, v_s(0) = v_s^0$ and $\hat{v}_s(0) = \hat{v}_s^0$,
- Additional velocities $\{w_f, w_s\} \in \{w_f^D + V_{f,w}^0\} \times \{w_s^D + V_{s,w}^0\}$ with $w_f(0) = w_f^0$ and $w_s(0) = w_s^0$,
- Displacements $\{u_f, \hat{u}_f, u_s, \hat{u}_s\} \in \{u_f^D + V_{f,u}^0\} \times \{\hat{u}_f^D + \hat{V}_{f,\hat{u}}^0\} \times \{u_s^D + V_{s,u}^0\} \times \{\hat{u}_s^D + \hat{V}_{s,\hat{u}}^0\}$ with $u_f(0) = u_f^0, \hat{u}_f(0) = \hat{u}_f^0, u_s(0) = u_s^0$ and $\hat{u}_s(0) = \hat{u}_s^0$,
- Pressures $\{p_f, \hat{p}_f\} \in L_f^0 \times \hat{L}_f^0$,

such that for $t \in I_T$ and $\alpha_w > 0$ holds:

$$\begin{aligned} & (\chi_f \rho_f \partial_t v_f, \psi_f^v) + (\chi_f \rho_f (v_f \cdot \nabla) v_f, \psi_f^v) \\ & + (\chi_f \sigma_f, \nabla \psi_f^v) - (\chi_f g_f n_f, \psi_f^v) - (\chi_f \rho_f f_f, \psi_f^v) \\ & = 0 \quad \forall \psi_f^v \in V_{f,v}^0, \end{aligned} \tag{32}$$

$$\begin{aligned} & (\hat{\chi}_f \hat{J} \hat{\rho}_f \partial_t \hat{v}_f, \hat{\psi}_f^v) + \hat{\chi}_f (\hat{\rho}_f \hat{J} (\hat{F}^{-1} (\hat{v}_f - \partial_t \hat{A}) \cdot \widehat{\nabla}) \hat{v}_f, \hat{\psi}_f^v) \\ & + (\hat{\chi}_f \hat{J} \hat{\sigma}_f \hat{F}^{-T}, \widehat{\nabla} \hat{\psi}_f^v) - (\hat{\chi}_f \hat{g}_f \hat{n}_f, \hat{\psi}_f^v) - (\hat{\chi}_f \hat{\rho}_f \hat{J} \hat{f}_f, \hat{\psi}_f^v) \\ & = 0 \quad \forall \hat{\psi}_f^v \in \hat{V}_{f,\hat{v}}^0, \end{aligned} \tag{33}$$

$$\begin{aligned} & (\chi_s J \rho_s \partial_t v_s, \psi_s^v) + (\chi_s J \rho_s (v_s \cdot \nabla) v_s, \psi_s^v) \\ & + (\chi_s \sigma_s, \nabla \psi_s^v) - (\chi_s J \rho_s f_s, \psi_s^v) \\ & = 0 \quad \forall \psi_s^v \in V_s^0, \end{aligned} \tag{34}$$

$$\begin{aligned} & (\hat{\chi}_s \hat{\rho}_s \partial_t \hat{v}_s, \hat{\psi}_s^v) + (\hat{\chi}_s \hat{J} \hat{\sigma}_s \hat{F}^{-T}, \widehat{\nabla} \hat{\psi}_s^v) - (\hat{\chi}_s \hat{\rho}_s \hat{f}_s, \hat{\psi}_s^v) \\ & = 0 \quad \forall \hat{\psi}_s^v \in \hat{V}_s^0, \end{aligned} \tag{35}$$

$$\chi_f \rho_f (\partial_t u_f + (w_f \cdot \nabla) u_f - w_f, \psi_f^u) = 0 \quad \forall \psi_f^u \in V_f^0, \tag{36}$$

$$(\hat{\chi}_f \widehat{\sigma}_{\text{mesh}}, \widehat{\nabla} \hat{\psi}_f^u) = 0 \quad \forall \hat{\psi}_f^u \in \hat{V}_{f,\hat{u},\hat{\Gamma}_{i,A}}^0, \tag{37}$$

$$\chi_s \rho_s (\partial_t u_s + (w_s \cdot \nabla) u_s - w_s, \psi_s^u) = 0 \quad \forall \psi_s^u \in V_s^0, \tag{38}$$

$$\hat{\chi}_s \hat{\rho}_s (\partial_t \hat{u}_s - \hat{v}_s, \hat{\psi}_s^u) = 0 \quad \forall \hat{\psi}_s^u \in \hat{L}_s, \tag{39}$$

$$\chi_f (\alpha_w \nabla w_f, \nabla \psi_f^w) = 0 \quad \forall \psi_f^w \in V_f^0, \tag{40}$$

$$\chi_s (v_s - w_s, \psi_s^w) = 0 \quad \forall \psi_s^w \in L_s, \tag{41}$$

$$(\chi_f \text{div } v_f, \psi_f^p) = 0 \quad \forall \psi_f^p \in L_f^0, \tag{42}$$

$$(\hat{\chi}_f \widehat{\text{div}} (\hat{J} \hat{F}^{-1} \hat{v}_f), \hat{\psi}_f^p) = 0 \quad \forall \hat{\psi}_f^p \in \hat{L}_f^0, \tag{43}$$

Let us understand the meaning of all the twelve equations in Problem 4, which is divided into seven parts. In part I, Eqs. (32) and (33) are the Navier-Stokes equations described in Eulerian coordinates and in the ALE framework. Then, in part II and IV, the first order system presented in Problem 2 is used. Consequently, the first equations (Eulerian and secondly in Lagrangian coordinates) are given here in part II. We notice in the Eulerian structure that we deal with an additional (nonstandard) convection term in Eq. (34) due to the transformation from the Lagrangian system. In the third part, we find transformations related to the fluid problems. Here, the first Eq. (36) comes from the IPS whereas the second Eq. (37) is the well-known moving-mesh PDE for ALE problems. Next, in part IV, the second equations of the elasticity system are given (therefore, related to part II). The next two parts V and VI, Eqs. (40) and (41), define the additional velocity variable w , which is only required in the Eulerian domain. Finally, the incompressibility condition of the fluid is expressed in part VII.

In Problem 4, the characteristic functions in $\widehat{\Omega}_{f,A}$ and $\widehat{\Omega}_{s,A}$ are defined as

$$\hat{\chi}_f := \begin{cases} 1, & \hat{x} \in \widehat{\Omega}_{f,A}, \\ 0, & \hat{x} \in \widehat{\Omega}_{s,A} \cup \widehat{\Gamma}_{i,A}, \end{cases} \quad \text{and} \quad \hat{\chi}_s := 1 - \hat{\chi}_f. \tag{44}$$

Specifically, the cells that belong to the ALE domain are simply marked in the fixed reference configuration because it is clear where the fluid and the structure are located thanks to the interface-tracking character of ALE. However, in the Eulerian domain it is a bit more complicated to identify the structure. Here, the characteristic functions in Ω_f and Ω_s are

defined as

$$\chi_f := \begin{cases} 1, & x - u \in \widehat{\Omega}_{f,E}, \\ 0, & x - u \in \widehat{\Omega}_{s,E} \cup \widehat{\Gamma}_{i,E}, \end{cases} \quad \text{and} \quad \chi_s = 1 - \chi_f. \quad (45)$$

Details are provided elsewhere [35].

Remark 5 (Mesh motion model of ALE) In the EALE method, the mesh motion model $\widehat{\sigma}_{\text{mesh}}$ of the ALE sub-framework is based on a linear elastic mesh motion (e.g., [52–56]) model because we aim to model moderate deflections with the help of the ALE coordinates; thus we expect no fluid mesh distortion in the ALE domain.

Remark 6 (Coupling conditions for fluid-structure interaction) As always in variational monolithically-coupled FSI, the coupling conditions are hidden in the test spaces and their implicit definition. Specifically, they read on the FSI-interface in strong form

$$v_f = v_s \quad \text{and} \quad \sigma_f(v, p)n_f = F \Sigma_s(u)n_s. \quad (46)$$

Remark 7 (Coupling conditions for coupling ALE with Eulerian) The coupling conditions to couple the ALE framework with the fully Eulerian framework on the EALE-interface are given by

$$\widehat{u}_{f,A} = u_{f,E} = 0, \quad (47)$$

$$\partial_n \widehat{u}_{f,A} = \partial_n u_{f,E} = 0, \quad (48)$$

$$\widehat{\sigma}_{f,A} \widehat{n}_{f,A} = \sigma_{f,E} n_{f,E}. \quad (49)$$

A deeper discussion is provided in [9].

Remark 8 (Mass conservation) We shall give a brief account to mass conservation because this is a well-known difficulty and often asked when using interface-capturing techniques. This is strongly-related to the signed distance function property, which needs to remain valid for long-time computations. For numerical validations, we refer the reader to [33,35].

Remark 9 (Signed distance function property) Even though reinitialization is not necessary in our framework, it is often being asked. In fact, although the interface-capturing-function is initialized as a signed distance function, it is not for sure it remains so. However, in many situations it is preferable to have a signed distance function throughout the numerical simulation. The reasons are that velocity extension methods can be employed successfully, a possibly given thickness of the interface remains valid, and finally, that the level-set function behaves well near the interface [57]. To ensure the signed-distance property, the interface-capturing-function needs to be reinitialized. For various methods and explication, we refer the reader to the level-set literature. For explicit usage of reinitialization in terms of fully Eulerian fluid-structure interaction, we refer to [37].

3.1 Discretization

In the proposed method, each sub-system is discretized with standard tools. A deeper discussion for our specific fully Eulerian and ALE codes is provided in [35] and [43,44].

We briefly summarize the basic steps in the following. The discretization of the continuous Problem 4 is based on the Rothe method; i.e., the equations are first discretized in time via a one-step- θ scheme. In particular, the backward Euler scheme and the shifted Crank-Nicolson scheme [58] can be represented as such schemes. Afterwards a Galerkin finite element scheme is used for spatial discretization. Specifically, the computational domain is triangulated into quadrilaterals. In the Eulerian sub-framework, seven solution variables need to be discretized:

$$v_f, v_s, w_f, w_s, u_f, u_s \in Q_2^c, \quad p_f \in P_1^{dc}.$$

In the ALE sub-framework, the problem requires discretization of five solution variables:

$$\widehat{v}_f, \widehat{v}_s, \widehat{u}_f, \widehat{u}_s \in Q_2^c, \quad \widehat{p}_f \in P_1^{dc}.$$

The definitions of the finite element spaces can be found in the standard literature [59,60]. In particular, the Q_2^c/P_1^{dc} element used for the fluid part is inf-sup stable and locally mass conserving. Consequently, no pressure stabilization à la PSPG [14] is necessary.

The nonlinear fully-discretized system is solved in each time step by Newton's method in which the Jacobian matrix is computed using analytical expressions [61,43,35]. For a deeper discussion on the numerics how to solve our monolithically-coupled fluid-structure interaction problems, we refer the reader to [43,35]. Moreover, the pure hyperbolic terms in the Eulerian structure are stabilized by adding some diffusion as presented in [35]. A more advanced technique such as a streamline upwind Petrov-Galerkin (SUPG) [62] is planned as future task. Finally, the specific quadrature rules in cells which are intersected by the interface is detailed in [35]. Furthermore, we refer to Belytschko et al. [63], who give quite useful remarks on numerical integration. In fact, we use a comparable algorithm for numerical integration as proposed by Moes et al. [64].

4 Numerical tests: an elastic beam in a fluid flow with elastic outer walls

The EALE framework 4 is validated with the help of modified FSI benchmark configurations which are based on suggestions by Hron and Turek [30,65]. Two settings in a laminar flow regime with different inflow velocity profiles are presented. The first example leads to a steady-state with a low Reynolds number and it is compared to results obtained by using the steady-state formulation presented elsewhere [9].

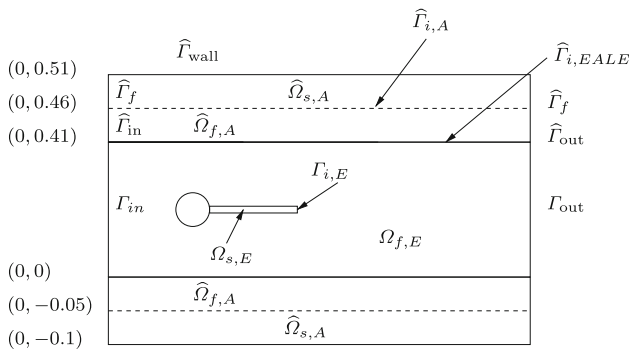


Fig. 2 Flow around cylinder with elastic beam and outer elastic walls with circle-center $C = (0.2, 0.2)$ and radius $r = 0.05$. Specifically, the Eulerian framework is employed in the ‘non-hat’ domains whereas the ‘hat’ regions are described in ALE coordinates

In the second example, a challenging nonstationary test case is considered. For each of the both test cases, two different values of $\mu_{wall} = 5 \times 10^5$ and $5,000 \times 10^5 \text{ kgm}^{-1}\text{s}^{-2}$ are utilized in which the elastic walls move significantly for the first choice $\mu_{wall} = 5 \times 10^5 \text{ kgm}^{-1}\text{s}^{-2}$.

Configuration

The computational domain has length $L=1.15$ m and total height $H=0.61$ m (with a channel width for the fluid $H_f=0.41$ m). The circle center is positioned at $C=(0.2, 0.2)$ m with radius $r=0.05$ m. The elastic beam has length $l=0.35$ m and height $h=0.02$ m. The right lower end is positioned at $(0.6, 0.19)$ m, and the left end is attached to the circle. At the top and the bottom, elastic structures are supplemented as displayed in Fig. 2. Specifically, the Eulerian framework is employed in the ‘non-hat’ domains whereas the ‘hat’ regions are described in ALE coordinates. Consequently, the advantages of both methods are combined: modeling large deflections inside the domain with the Eulerian approach and movement of elastic walls thanks to the ALE method.

Boundary conditions

The velocity and the displacements are kept free on the top and bottom boundary Γ_{wall} to allow them to move. On the left boundary parts Γ_{in} and $\widehat{\Gamma}_{in}$, the displacements are fixed by homogenous Dirichlet conditions and a Dirichlet inflow velocity profile is prescribed on Γ_{in} . The velocity is zero on $\widehat{\Gamma}_{in}$. On the right boundary (outflow boundary Γ_{out} and $\widehat{\Gamma}_{out}$), the displacements are fixed and the velocity is kept free (do-nothing condition). This choice leads in particular to pressure normalization [66].

Inflow profile

A parabolic inflow velocity profile is given on Γ_{in} by

$$v_f(0, y) = 1.5\bar{U} \frac{4y(H_f - y)}{H_f^2}, \quad \bar{U} = \underbrace{0.2}_{\text{mod. FSI 1}}, \underbrace{1.0 \text{ ms}^{-1}}_{\text{mod. FSI 2}}.$$

For the non-steady tests one should start with a smooth increase of the velocity profile in time. We use

$$v_f(t; 0, y) = \begin{cases} v_f(0, y) \frac{1 - \cos(\frac{\pi}{2}t)}{2} & \text{if } t < 2.0\text{s} \\ v_f(0, y) & \text{otherwise.} \end{cases}$$

Parameters

We choose for our computation the following parameters in the Eulerian framework in Ω_E . For the fluid we use $\rho_{f,E} = 10^3 \text{ kg m}^{-3}$, $\nu_{f,E} = 10^{-3} \text{ m}^2 \text{ s}^{-1}$. The elastic structure (STVK material) is characterized by $\rho_{s,E} = 10^3 \text{ kg m}^{-3}$ (for the first test case) or $\rho_{s,E} = 10^4 \text{ kg m}^{-3}$ (for the second test case), $\nu_{s,E} = 0.4$, $\mu_{s,E} = 5 \times 10^5 \text{ kg m}^{-1} \text{ s}^{-2}$. The value of the thickness parameter for the interface in the Eulerian approach is chosen as 10^{-12} (thus a sharp interface is used). For a more detailed explication, we refer the reader to [35].

In the ALE framework in $\widehat{\Omega}_A$, we choose $\rho_{f,A} = 10^3 \text{ kg m}^{-3}$, $\nu_{f,A} = 10^{-3} \text{ m}^2 \text{ s}^{-1}$. The elastic structure (STVK material) is characterized by $\rho_{s,A} = 10^3 \text{ kg m}^{-3}$, $\nu_{s,A} = 0.4$. The Lamé coefficient $\mu_{s,A}$ takes two different values to observe different movements of the outer elastic walls: $\mu_{wall} = 5 \times 10^5$ and $5,000 \times 10^5 \text{ kgm}^{-1} \text{ s}^{-2}$.

Quantities of interest and their evaluation

- (1) x - and y -deflection of the beam at $A(t)$ (with $A(0) = (0.6, 0.2)$).
- (2) x - and y -deflection of the wall at $B(t)$ (with $B(0) = (0.2, 0.51)$).
- (3) The forces exerted by the fluid on the whole body, i.e., drag force F_D and lift force F_L on the rigid cylinder and the elastic beam. They form a closed path in which the forces can be computed with the help of line integration. For the Eulerian part, we use

$$(F_D, F_L) = \int_{\text{cylinder}, f, E} \sigma_f \cdot n_f ds + \int_{\text{cylinder}, s, E} \sigma_s \cdot n_s ds, \quad (50)$$

in which ‘cylinder,s,E’ denotes the circle path where the beam is attached to the cylinder.

For the modified FSI 2 test, we display the mean value and the amplitude.

4.1 Discussion of results: modified FSI 1 benchmark

For this test, the implicit Euler time-stepping scheme is used with $k=0.01$ s and $T=30$ s (total time). In addition, we compare the results to the standard FSI 1 simulation, without any additional elastic boundaries (configuration and parameters

Table 1 Results for FSI 1 in EALE coordinates with elastic walls with $\mu_{wall} = 5.0 \times 10^5$

Level	DoF	u_y^{beam}	u_y^{wall}	F_D
0	5445	111.70	9.30	10.10
1	20988	4.70	13.24	10.10
2	82368	6.39	13.06	10.29
Ref [9]	82368	7.04	12.94	9.66
ALE	57904	8.19	–	15.33

The values for u_y^{beam} and u_y^{wall} are scaled by 10^{-4} . In last row, the results of the standard FSI 1 benchmark computed with the ALE method and linear-elastic moving-mesh method are given

Table 2 Results for FSI 1 in EALE coordinates with elastic walls with $\mu_{wall} = 5.0 \times 10^8$

Level	DoF	u_y^{beam}	u_y^{wall}	F_D
0	5445	111.36	0.0895	10.02
1	20988	4.51	0.0134	10.29
2	82368	6.40	0.0130	10.44
Ref [9]	82368	7.15	0.0129	9.82
ALE	57904	8.19	–	15.33

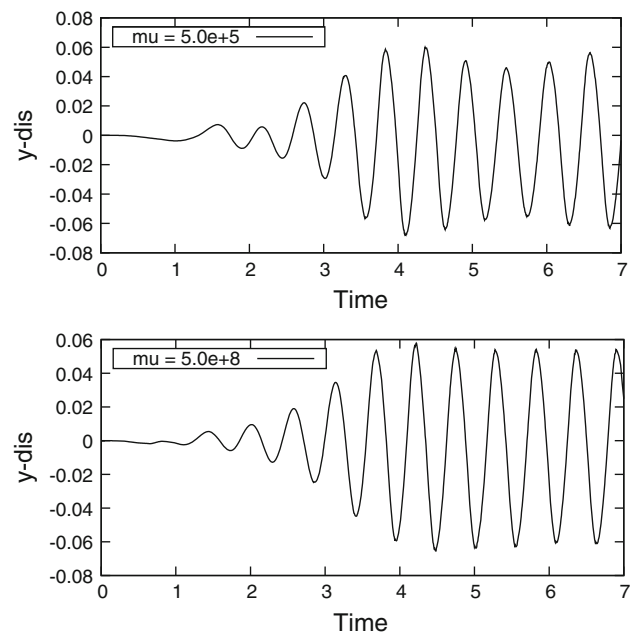
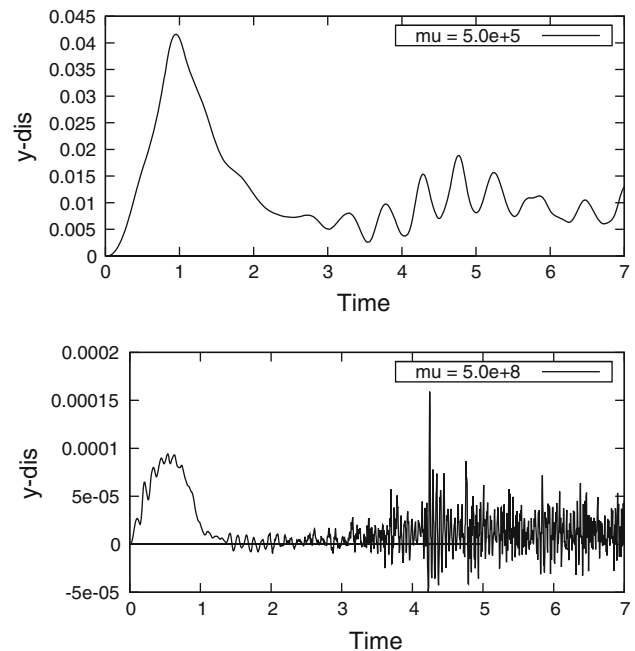
The values for u_y^{beam} and u_y^{wall} are scaled by 10^{-4} . In last row, the results of the standard FSI 1 benchmark computed with the ALE method and linear-elastic moving-mesh method are given

taken from [65]), conducted with help of the code (using a linear-elastic mesh-moving model) presented in [46].

Comparing the results, we first notice that the findings on level 0 (the coarsest mesh) should be interpreted carefully because the Eulerian method needs a fine mesh to work with sufficient accuracy. Therefore, the u_y^{beam} -values differ quite significantly from the findings on level 1 and 2. All values on level 2 (the finest mesh) show good agreement with the reference findings as displayed in the Tables 1 and 2. Finally, comparing the modified FSI 1 results to the standard benchmark (last row in both tables), we see the influence by adding the additional elastic boundaries. The smoother the elastic boundary, the smaller the deformation of the beam. In the limit $\mu_{wall} = \infty$ (which corresponds to the original FSI 1 benchmark without boundaries), we observe the highest beam deformation. This is reasonable because the beam-deflection is induced in the non-symmetry of the configuration. However, the smoother the elastic boundary, less force acts on the beam.

4.2 Discussion of results: modified FSI 2 benchmark test

The only two changes to the previous test case is a higher structure density $\rho_{s,E} = 10^4 \text{ kg m}^{-3}$ and a higher inflow profile $\bar{U} = 1.0 \text{ ms}^{-1}$. This numerical example is challenging because without any elastic structures the flow regime

**Fig. 3** Modified FSI 2 test on the finest mesh: Comparison of the deflection at $A(t)$ versus time for $\mu_{wall} = 5.0 \times 10^5$ (top) and $\mu_{wall} = 5.0 \times 10^8$ (bottom)**Fig. 4** Modified FSI 2 test on the finest mesh: comparison of the deflection at $B(t)$ versus time for $\mu_{wall} = 5.0 \times 10^5$ (top) and $\mu_{wall} = 5.0 \times 10^8$ (bottom). Using a very stiff wall as shown at right, the deflection of $B(t)$ consists mainly of noise around zero displacement. Remark: The vertical axis are in different scales in order to detect the noise in the figure at the bottom

would yield a steady-state solution since the Reynolds number is too low. Thus, the development of dynamic behavior is only due to the interaction of fluid and elastic beam.

Table 3 Results for the modified FSI 2 benchmark with outer elastic structures and $\mu^{wall} = 5.0 \times 10^5$

Dof	$k[10^{-3}]$	$u_x^{beam}(A)$	$u_y^{beam}(A)$	$u_x^{wall}(A)$	$u_y^{wall}(A)$
20988	5	-4.92 ± 4.86	-4.33 ± 44.42	-8.23	+4.1
82368	5	-8.63 ± 8.10	-3.28 ± 59.23	-8.30	+4.2
20988	2.5	-4.89 ± 4.82	-4.57 ± 43.75	-7.87	+3.9
82368	2.5	-7.69 ± 7.11	-4.01 ± 60.01	-7.87	+4.0
20988	1.25	-4.83 ± 4.74	-4.68 ± 43.32	-7.50	+3.8
82368	1.25	-7.22 ± 6.64	-4.34 ± 60.38	-7.50	+3.8

The mean value and amplitude are given for $u_x^{beam}(10^{-3} \text{ m})$, $u_y^{beam}(10^{-3} \text{ m})$. Moreover, the maximal deflections $u_x^{wall}(10^{-6} \text{ m})$, $u_y^{wall}(10^{-5} \text{ m})$ at the point $B(t)$ is displayed. The frequencies $f_1(\text{s}^{-1})$ and $f_2(\text{s}^{-1})$ of u_x^{beam} and u_y^{beam} vary in a range of 3.49–3.88 and 1.86–1.88, respectively. After the pick displacements around time step $t = 1 \text{ s}$, the walls show regular oscillations, where the wall x -displacements vary with an amplitude of 1.25×10^{-3} and the wall y -displacements vary with an amplitude of 3.09×10^{-3}

Table 4 Results for the modified FSI 2 benchmark with outer elastic structures and $\mu^{wall} = 5.0 \times 10^8$

Dof	$k[10^{-3}]$	$u_x^{beam}(A)$	$u_y^{beam}(A)$
20988	5	-4.53 ± 4.41	-2.72 ± 44.52
82368	5	-7.46 ± 6.92	-3.34 ± 57.98
20988	2.5	-4.52 ± 4.45	-2.93 ± 44.31
82368	2.5	-6.89 ± 6.50	-1.89 ± 55.70
20988	1.25	-4.31 ± 4.23	-4.48 ± 44.24
82368	1.25	-6.86 ± 6.42	-1.92 ± 55.20

The mean value and amplitude are given for two quantities of interest: $u_x(10^{-3} \text{ m})$, $u_y(10^{-3} \text{ m})$. The frequencies $f_1(\text{s}^{-1})$ and $f_2(\text{s}^{-1})$ of u_x^{beam} and u_y^{beam} vary in a range of 3.87–4.02 and 1.85–1.88, respectively.

A careful resolution of the interface-force-balance is therefore necessary in each time step (well known as strong coupling).

We compare again two settings in which the Lamé coefficient of the outer ALE structure is varied. First, a smooth structure using $\mu_{s,ALE} = 5.0 \times 10^5 \text{ kg m}^{-1} \text{ s}^{-2}$ is investigated, leading to significant movement of the outer walls. Second, the structure stiffness is increased to $\mu_{s,ALE} = 5.0 \times 10^8 \text{ kg m}^{-1} \text{ s}^{-2}$ such that the boundaries are almost rigid. The second-order shifted Crank-Nicolson scheme using different sizes of time steps is employed in this test case. In comparison to the standard Crank-Nicolson scheme, it can be used for long-term computations as theoretically proven by Rannacher [58]. Specifically, numerical comparisons for fluid-structure interaction have been undertaken by Wick [67].

The mean value of the drag varies in a range of 137–157 and its amplitude 90–127. The mean of the lift varies in a range of 19–38 and its amplitude 89–147.

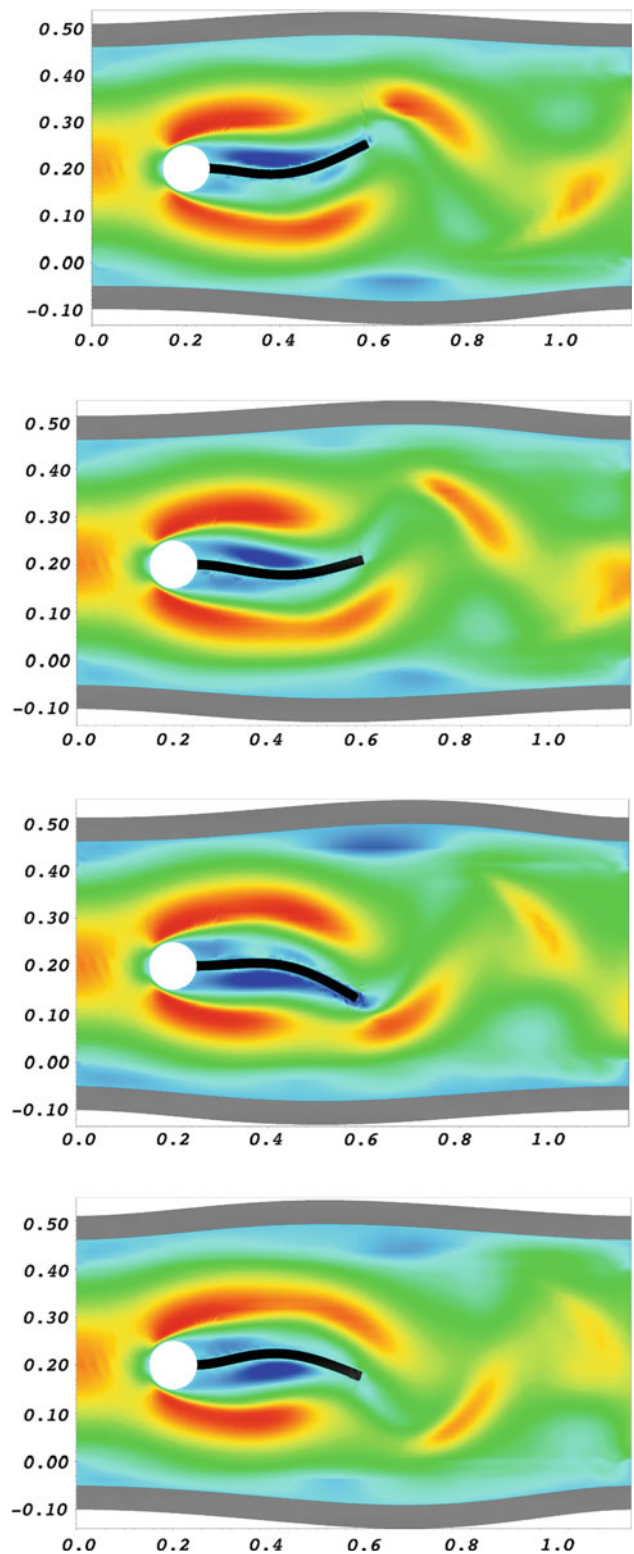


Fig. 5 Modified FSI 2 test with smooth elastic walls in the physical domain using $\mu_{wall} = 5.0 \times 10^5$ (smooth elastic boundaries). The elastic beam modeled in Eulerian coordinates is displayed in black. The outer elastic walls modeled in ALE coordinates are displayed in grey. The fluid is represented by the x -velocity profile with highest velocity in red. Different time steps $t = 3.89, 3.985, 4.1, 4.225 \text{ s}$ from top to bottom are displayed

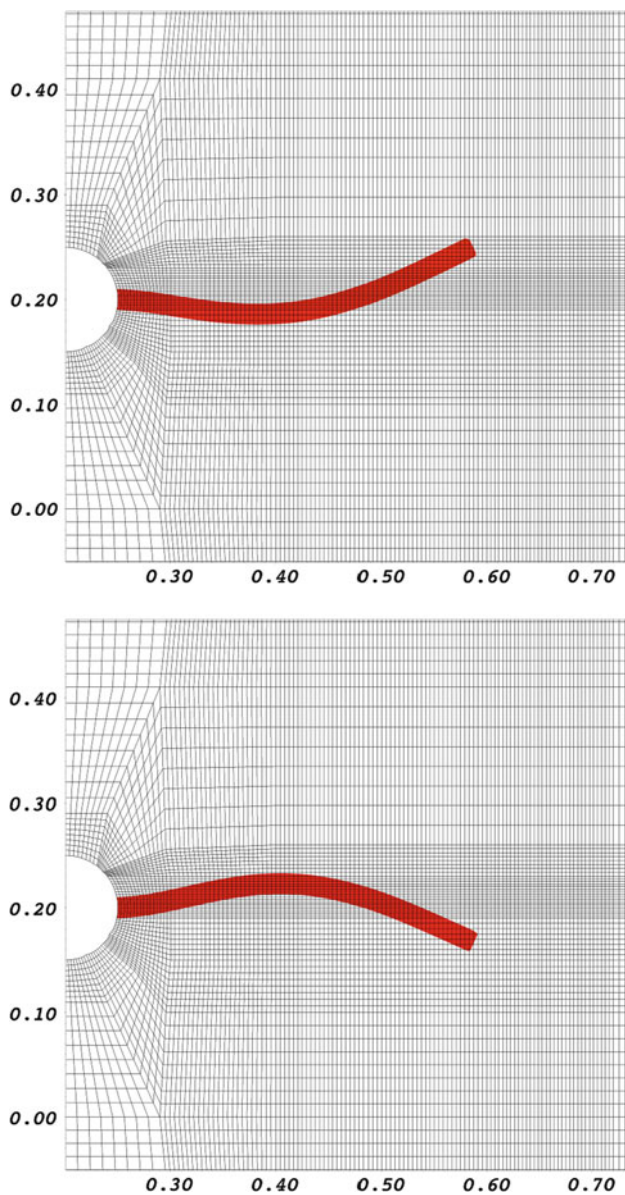


Fig. 6 Modified FSI 2 test with smooth elastic walls in the physical domain using $\mu_{\text{wall}} = 5.0 \times 10^5$ (smooth elastic boundaries). Focus on the elastic beam (in red), which is allowed to intersect mesh cells. Two time steps $t = 3.89, 4.225$ are displayed

In particular, the test case with a smooth wall, substantiates the performance of our proposed method for fully non-stationary fluid-structure interaction. The pick values of wall movement are provided in Fig. 4 and Table 3.

In contrast to a smooth wall, we omit the wall displacements for the stiff case because only noise (as expected) around zero is observed as shown in Fig. 3. Comparing the results in Table 3 and 4, we observe that the stiffness of the wall has negligible influence on the displacements of the elastic beam. Furthermore, we identify comparable values for the drag and lift forces—the details for the second test case are

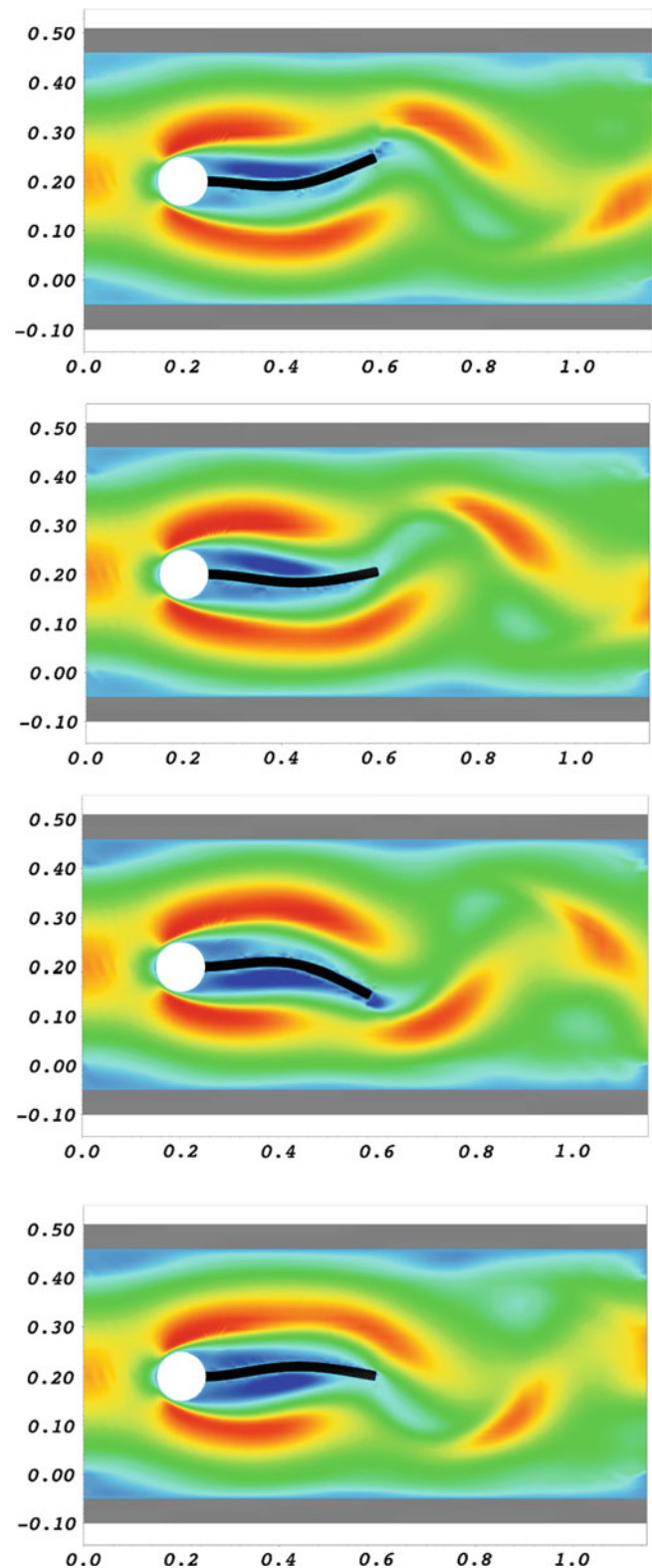


Fig. 7 Modified FSI 2 test with stiff elastic walls in the physical domain using $\mu_{\text{wall}} = 5.0 \times 10^8$ (very stiff elastic boundaries). The elastic beam modeled in Eulerian coordinates is displayed in black. The outer elastic walls modeled in ALE coordinates are displayed in grey. The fluid is represented by the x -velocity profile with highest velocity in red. Different time steps $t = 3.72, 3.835, 3.975, 4.125$ s from top left to bottom right are displayed

omitted for the convenience of the reader. Moreover, the values for the stiff wall are already known from computations without elastic walls [35]. Moreover, we monitor time convergence as shown in Tables 3 and 4. However, it can be inferred from our results on two different mesh levels that spatial discretization has much more influence on the maximal amplitudes. Future studies should focus on computations on very fine meshes to identify the maximal amplitudes for this test case. (Despite this missing study, we nevertheless believe that our method is validated because a spatial mesh convergence study was made in Example 4.1). The dynamics are illustrated in the Figs. 5, 6, and 7 with a zoom-in on the intersecting elastic beam in Fig. 6.

5 Conclusions

In this study, the EALE method as a specific realization of the FSITICT (the FSI version of the MITICT) approach has been validated for fluid-structure computations. As shown, this method provides the possibility to couple deformations of elasticity described in different coordinates. The performance was demonstrated by some benchmark tests. In future studies, it is planned to apply the framework to problems in computational medicine.

Acknowledgments I am grateful to Rolf Rannacher (Heidelberg) for the possibility to start working on this topic. Since I moved in the meantime to ICES (UT Austin), many thanks to Mary F. Wheeler (Center for Subsurface Modeling at ICES, Austin) for the possibility to finish this work. Moreover, I thank Marie-Cécile Wick and Elisa A. M. Wick for their patience because final preparation and the revised version were pure weekend work. Finally, I would like to thank both reviewers for their valuable comments which improved a lot the value of this study.

References

- Tezduyar T, Takizawa K, Moorman C, Wright S, Christopher J (2010) Space-time finite element computation of complex fluid-structure interaction. *Int J Numer Methods Fluids* 64:1201–1218
- Tezduyar T (2001) Finite element methods for flow problems with moving boundaries and interfaces. *Arch Comput Methods Eng* 8(2):83–130
- Donéa J, Fasoli-Stella P, Giuliani S (1977) Lagrangian and Eulerian finite element techniques for transient fluid-structure interaction problems. In: *Trans. 4th international conference on structural mechanics in reactor technology*, p B1/2
- Hirt C, Amsden A, Cook J (1974) An arbitrary Lagrangian–Eulerian computing method for all flow speeds. *J Comput Phys* 14:227–253
- Hughes T, Liu W, Zimmermann T (1981) Lagrangian–Eulerian finite element formulation for incompressible viscous flows. *Comput Methods Appl Mech Eng* 29:329–349
- Noh W (1964) A time-dependent two-space-dimensional coupled Eulerian–Lagrangian code. Academic Press, New York, pp 117–179
- Dunne T (2006) An Eulerian approach to fluid-structure interaction and goal-oriented mesh adaptation. *Int J Numer Methods Fluids* 51:1017–1039
- Liu C, Walkington N (2001) An Eulerian description of fluids containing visco-elastic particles. *Arch Rat Mech Anal* 159: 229–252
- Wick T (2012) Coupling of fully Eulerian with arbitrary Lagrangian–Eulerian coordinates for fluid-structure interaction. Under review in *CMAME*
- Tezduyar T (2006) Interface-tracking and interface-capturing techniques for finite element computation of moving boundaries and interfaces. *Comput Methods Appl Mech Eng* 195:2983–3000
- Akin JE, Tezduyar T, Ungor M (2007) Computation of flow problems with the mixed interface-tracking/interface-capturing technique (MITICT). *Comput Fluids* 36:2–11
- Cruchaga M, Celentano D, Tezduyar T (2007) A numerical model based on the mixed interface-tracking/ interface-capturing technique (MITICT). *Int J Numer Methods Fluids* 54:1021–1030
- Takizawa K, Spielman T, Tezduyar T (2011) Space-time FSI modeling and dynamical analysis of spacecraft parachutes and parachute clusters. *Comput Mech* 48:345–364
- Tezduyar T (1992) Stabilized finite element formulations for incompressible flow computations. *Adv Appl Mech* 28:1–44
- Tezduyar T, Behr M, Liou J (1992) A new strategy for finite element computations involving moving boundaries and interfaces - the deforming-spatial-domain/space-time procedure: I. the concept and the preliminary numerical tests. *Comput Methods Appl Mech Eng* 94:339–351
- Tezduyar T, Behr M, Mittal S, Liou J (1992) A new strategy for finite element computations involving moving boundaries and interfaces: the deforming-spatial-domain/space-time procedure: II. Computation of free-surface flows, two-liquid flows, and flows with drifting cylinders. *Comput Methods Appl Mech Eng* 94:353–371
- Tezduyar T, Sathe S, Stein K (2006) Solution techniques for the fully discretized equations in computation of fluid-structure interaction with space-time formulations. *Comput Methods Appl Mech Eng* 195(41–43):5743–5753
- Tezduyar T, Aliabadi S (2000) EDICT for 3D computation of two-fluid interfaces. *Comput Methods Appl Mech Eng* 190:403–410
- Tezduyar T, Aliabadi S, Behr M (1998) Enhanced-discretization interface-capturing technique (EDICT) for computation of unsteady flows with interfaces. *Comput Methods Appl Mech Eng* 155:235–248
- Asterino M, Gerbeau JF, Pantz O, Traoré KF (2009) Fluid-structure interaction and multi-body contact: application to aortic valves. *Comput Methods Appl Mech Eng* 198:3603–3612
- Baaijens F (2001) A fictitious domain/mortar element method for fluid-structure interaction. *Int J Numer Methods Fluids* 35(7):743–761
- Caniceros HD, Fisher JE, Roma AM (2009) Efficient solutions to robust, semi-implicit discretizations of the immersed boundary method. *J Comput Phys* 228:7137–7158
- van Loon R, Anderson P, van de Vosse F (2006) A fluid-structure interaction method with solid-rigid contact for heart valve dynamics. *J Comput Phys* 217:806–823
- Peskin C (2002) *The immersed boundary method*. Acta numerica 200. Cambridge University Press, Cambridge
- Santos NDD, Gerbeau JF, Bourgat J (2008) A partitioned fluid-structure algorithm for elastic thin valves with contact. *Comput Methods Appl Mech Eng* 197(19–20):1750–1761
- Hron J (2001) Fluid structure interaction with applications in biomechanics. Ph.D. thesis. Charles University Prague
- Hron J, Turek S (2006) A monolithic FEM/multigrid solver for ALE formulation of fluid structure with application in biomechanics. Springer, Berlin, pp 146–170

28. Huebner B, Walhorn E, Dinkler D (2004) A monolithic approach to fluid structure interaction using space-time finite elements. *Comput Methods Appl Mech Eng* 193(23–26):2087–2104. doi:10.1016/j.cma.2004.01.024
29. Bazilevs Y, Calo VM, Hughes T, Zhang Y (2008) Isogeometric fluid-structure interaction: theory, algorithms, and computations. *Comput Mech* 43:3–37
30. Bungartz HJ, Schäfer M (2006) Fluid-structure interaction: modelling, simulation, optimization, lecture notes in computational science and engineering, vol. 53. Springer, Berlin
31. Tezduyar T, Sathe S (2007) Modeling of fluid-structure interactions with the space-time finite elements: solution techniques. *Int J Numer Methods Fluids* 54:855–900
32. Tezduyar T, Sathe S, Keedy R, Stein K (2006) Space-time finite element techniques for computation of fluid-structure interactions. *Comput Methods Appl Mech Eng* 195:2002–2027
33. Richter T (2012) A fully Eulerian formulation for fluid-structure interaction problems. *J Comput Phys* 233:227–240
34. Richter T, Wick T (2010) Finite elements for fluid-structure interaction in ALE and fully Eulerian coordinates. *Comput Methods Appl Mech Eng* 199:2633–2642
35. Wick T (2012) Fully Eulerian fluid-structure interaction for time-dependent problems. *Comput Methods Appl Mech Eng* 255:14–26. doi:10.1016/j.cma.2012.11.009
36. Cottet GH, Maitre E, Mileent T (2008) Eulerian formulation and level set models for incompressible fluid-structure interaction. *Math Modell Numer Anal* 42:471–492
37. He P, Qiao R (2011) A full-Eulerian solid level set method for simulation of fluid-structure interactions. *Microfluid Nanofluid* 11:557–567
38. Sugiyama K, Li S, Takeuchi S, Takagi S, Matsumoto Y (2011) A full Eulerian finite difference approach for solving fluid-structure interaction. *J Comput Phys* 230:596–627
39. Takagi S, Sugiyama K, Matsumoto Y (2012) A review of full Eulerian methods for fluid structure interaction problems. *J Appl Mech* 79(1):7
40. Zhao H, Freund J, Moser R (2008) A fixed-mesh method for incompressible flow-structure systems with finite solid deformations. *J Comput Phys* 227(6):3114–3140
41. Causin P, Gerbeau JF, Nobile F (2005) Added-mass effect in the design of partitioned algorithms for fluid-structure problems. *Comput Methods Appl Mech Eng* 194:4506–4527
42. Formaggia L, Quarteroni A, Veneziani A (2009) Cardiovascular mathematics: modeling and simulation of the circulatory system. Springer, Milano
43. Wick T (2011) Adaptive finite element simulation of fluid-structure interaction with application to heart-valve dynamics. Ph.D. thesis. University of Heidelberg
44. Wick T (2011) Fluid-structure interactions using different mesh motion techniques. *Comput Struct* 89(13–14):1456–1467
45. Davis TA, Duff IS (1997) An unsymmetric-pattern multifrontal method for sparse LU factorization. *SIAM J Matrix Anal Appl* 18(1):140–158
46. Wick T (2012) Solving monolithic fluid-structure interaction problems in arbitrary Lagrangian Eulerian coordinates with the deal.ii library. *Archive for Numerical Software*, accepted, Vol. 1, pp. 1–19, Preprint available at IWR Heidelberg
47. Bangerth W, Heister T, Kanschat G (2012) Differential equations analysis library
48. Adams RA (1975) Sobolev spaces. Academic Press, New York
49. Wloka J (1982) Partielle differentialgleichungen. B. G. Teubner, Stuttgart
50. Ciarlet PG (1984) Mathematical elasticity: three dimensional elasticity. North-Holland, Amsterdam
51. Sussman M, Smereka P, Osher S (1994) A level set approach for computing solutions to incompressible two-phase flow. *J Comput Phys* 114:146–159
52. Johnson AA, Tezduyar T (1994) Mesh update strategies in parallel finite element computations of flow problems with moving boundaries and interfaces. *Comput Methods Appl Mech Eng* 119:73–94
53. Sackinger PA, Schunk PR, Rao RR (2005) A Newton-Raphson pseudo-solid domain mapping technique for free and moving boundary problems: a finite element implementation. *J Comput Phys* 125(1):83–103
54. Stein K, Tezduyar T, Benney R (2003) Mesh moving techniques for fluid-structure interactions with large displacements. *J Appl Mech* 70:58–63
55. Tezduyar T, Aliabadi S, Behr M, Johnson A, Mittal S (1993) Parallel finite element computation of 3D flows. *Computer* 26:27–36
56. Tezduyar TE, Behr M, Mittal S, Johnson AA (1992) Computation of unsteady incompressible flows with the finite element methods space-time formulations, iterative strategies and massively parallel implementations, new methods in transient analysis, PVP-Vol. 246, AMD-Vol. 143, vol. 143, pp. 7–24. ASME, New York
57. Sethian J, Smereka P (2003) Level set methods for fluid interface. *Annual Review*
58. Rannacher R (1986) On the stabilization of the Crank-Nicolson scheme for long time calculations, University des Saarlandes, Preprint
59. Ciarlet PG (1987) The finite element method for elliptic problems, 2. pr. edn. North-Holland, Amsterdam
60. Girault V, Raviart PA (1986) Finite element method for the Navier-Stokes equations. Number 5 in computer series in computational mathematics. Springer, Berlin
61. Fernández F, Moubachir M (2005) A Newton method using exact Jacobians for solving fluid-structure coupling. *Comput Struct* 83:127–142
62. Brooks A, Hughes T (1982) Streamline upwind/Petrov-Galerkin formulations for convection dominated flows with particular emphasis on the incompressible Navier-Stokes equations. *Comput Methods Appl Mech Eng* 32(1–3):199–259
63. Belytschko T, Parimi C, Moes N, Sukumar N, Usui S (2003) Structured extended finite element methods for solids defined by implicit surfaces. *Int J Numer Methods Eng* 56:609–635
64. Moes N, Dolbow J, Belytschko T (1999) A finite element method for crack growth without remeshing. *Int J Numer Methods Eng* 46:131–150
65. Hron J, Turek S (2006) Proposal for numerical benchmarking of fluid-structure interaction between an elastic object and laminar incompressible flow. Springer, Berlin, pp 146–170
66. Heywood JG, Rannacher R, Turek S (1996) Artificial boundaries and flux and pressure conditions for the incompressible Navier-Stokes equations. *Int J Numer Methods Fluids* 22:325–352
67. Wick T (2011) Stability estimates and numerical comparison of second order time-stepping schemes for fluid-structure interactions. In: *Numerical mathematics and advanced applications 2011*. ENUMATH 2011 in Leicester, UK